Journal of Materials Chemistry A

Accepted Manuscript

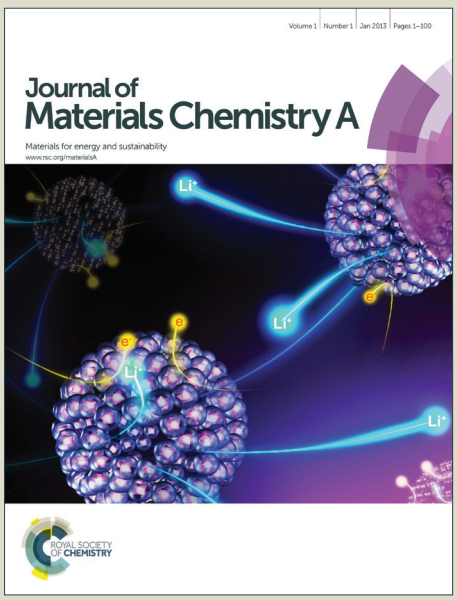

ROYAL SOCIETY OF CHEMISTRY

www.rsc.org/materialsA

Cite this: DOI: 10.1039/c0xx00000x

www.rsc.org/xxxxxx

COMMUNICATION

Mesoporous-assembled MnO_2 with large specific surface area

Gaini Zhang, Lijun Ren, Zhe Yan, Liping Kang, Zhibin Lei, Hua Xu, Feng Shi and Zong-Huai Liu*

Received (in XXX, XXX) Xth XXXXXXXXX 20XX, Accepted Xth XXXXXXXXX 20XX
DOI: 10.1039/b000000x

Mesoporous-assembled MnO_2 with large specific surface area was prepared by heating the delaminated MnO_2 nanosheet slurry with NH_4HSO_4 at 175 °C. When the molar ratio of NH_4HSO_4 to MnO_2 is 2.1, the obtained material had the largest specific surface area of 456 m^2 g^{-1}, which gives high specific capacitance of 281 F g^{-1} at a current density of 0.25 A g^{-1} and excellent cycling performance with about 1.9% loss after 2000 cycles.

Micro/nano-sized transition metal oxides with large specific surface area have received wide attention due to their potential applications in energy storage, catalysis, separation, and gas sensing.[1-3] Among the transition metal oxides with various valence states, the micro/nano-sized manganese oxides with large specific surface area have been confirmed to be one of the most promising pseudocapacitance electrode materials due to their high capacitance and activity/stability in neutral electrolyte system.[4,5] In order to improve the specific capacitance of the manganese oxide electrodes, the micro/nano-sized manganese oxide electrodes with both large specific surface area and high active sites are needed, which can be expected to exert the electric double layer capacitance from the large specific surface area and the pseudocapacitance from the high active site for redox reactions according to the capacitor storage mechanism.[6,7]

Research results indicate that the specific capacitance of manganese oxide electrodes is critically dependent on their effective specific surface area associated with the proper pore-size distribution and pore volume besides their crystalline structure.[8] Up to now, the micro/nano-sized manganese oxide electrodes with both large specific surface area and high active sites have been prepared by many methods, and these materials show good electrochemical properties.[9,10] By constructing more porous channels to obtaining "opened" structures, the hierarchical porous nanostructure with a specific surface area of 269 m^2 g^{-1} is assembled from ultrathin MnO_2 nanoflakes in an ice bath.[11] The flower-like microsphere δ-MnO_2 with a specific surface area of 280 m^2 g^{-1} is obtained by hydrothermal treating a mixture solution of $KMnO_4$ and $(NH_4)_2SO_4$ at 90 ℃.[12] The mesoporous MnO_2 with an average pore size of 3-4 nm and a BET surface area of 429 m^2 g^{-1} can be obtained by the reaction between ethanol and $KMnO_4$ using cetyltrimethylammonium bromide as soft template.[13] Although manganese oxide electrodes with various structures and morphologies have been prepared via different routes, their specific surface area is lower than 290 m^2 g^{-1}. In addition, although hard/soft templates (e.g., SBA-15,[14] n-butanol,[15] P123,[11] etc.) can be used to prepare mesoporous-assembled MnO_2 with large specific surface area, the preparation process complicats and time-consuming. Therefore, developing a novel preparation technique for micro/nano-sized manganese oxide electrodes with both large specific surface area and high active site is needed not only for academic research, but also for developing advanced energy storage materials.

Herein, a novel preparation technique for micro/nano-sized manganese oxide electrodes with both large specific surface area and high active site was developed by heating the delaminated MnO_2 nanosheet slurry with NH_4HSO_4 at 175 °C (detailed preparation processes were given in ESI†), and the prepared mesoporous-assembled MnO_2 shows a large specific surface area of 456 m^2 g^{-1} and their particle size is about 5 nm. The mesoporous-assembled MnO_2 electrode shows good cycling stability with about 1.9 % loss after 2000 cycles at a current density of 2 A g^{-1}. To the best of our knowledge, this is the most effective way to mass-produced micro/nano-sized manganese oxides with a large specific surface area.

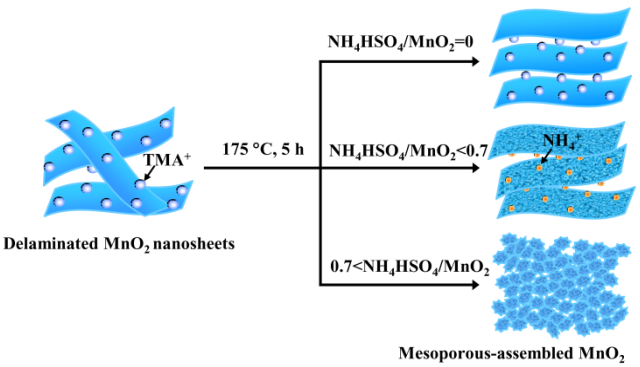

Scheme 1 Formation schematic illustration of the mesoporous-assembled MnO_2.

The novel fabrication process is schematically illustrated in Scheme 1. The delaminated MnO_2 nanosheets with a thickness of 0.45 nm are selected as a precursor because they have higher freedom degree than their assembled bulk and can be mixed uniformly with NH_4HSO_4. The formation process of the

mesoporous-assembled MnO_2 consists of three steps. Firstly, as the delaminated MnO_2 nanosheets are metastable state, they are reassembled by calcining at 175 ℃ without NH_4HSO_4 addition, and tetramethylammonium ions (TMA^+) intercalated manganese oxide with a basal spacing of 0.96 nm is formed.[16] Secondly, when the molar ratio of NH_4HSO_4/MnO_2 is below 0.7, the TMA^+ ions are exchanged with NH_4^+ ions originated from NH_4HSO_4, and NH_4^+ ions intercalated manganese oxide is obtained. Finally, NH_4^+ ions intercalated manganese oxide is converted to amorphous manganese oxide when the molar ratio further increases (NH_4HSO_4/MnO_2 > 0.7). The preparation process is supported by X-ray diffraction patterns of the obtained materials with different molar ratios of NH_4HSO_4/MnO_2 (Fig. 1).

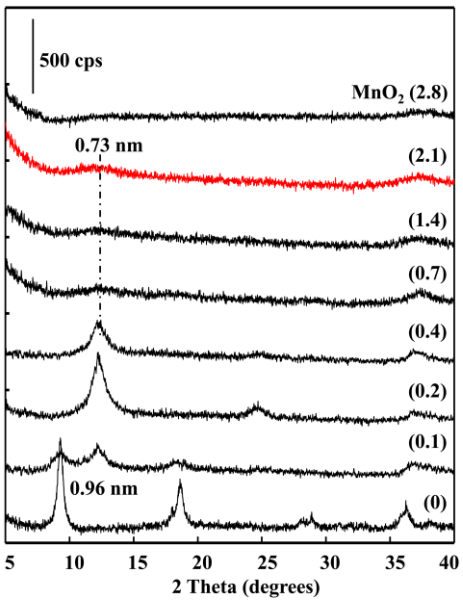

Fig. 1 XRD patterns of the mesoporous-assembled MnO_2 with different molar ratios of NH_4HSO_4/MnO_2.

The XRD pattern of the manganese oxide slurry gives only an amorphous halo (Fig. S1a†), scattering from the delaminated manganese oxide nanosheets aggregated irregularly.[17] The thickness of thin transparent platelets less than 0.5 nm are also observed (Fig. S1b†), suggesting that the layered manganese oxide is delaminated. The delaminated manganese oxide slurry calcined at 175 °C for 5 h, a typical layered structure with a basal spacing of 0.96 nm is obtained, corresponding to the intercalation of unhydrated TMA^+ ions into the interlayer. Increasing the molar ratios of NH_4HSO_4/MnO_2 (0.1-0.4), the basal spacing decreases to 0.73 from 0.96 nm although the layered structure remains, suggesting that an ion exchange reaction takes place and TMA^+ ions in the interlayer are exchanged with NH_4^+ ions released by NH_4HSO_4.[18] Further increase the molar ratios of NH_4HSO_4/MnO_2 (0.7-2.8), the XRD patterns of the obtained materials show broad peak in low intensity, suggesting that the obtained materials show nearly amorphous nature with smaller particle sizes.

The variation of TEM morphology also supports the reaction process (Fig. 2). In comparison with the morphology of the delaminated MnO_2 nanosheets (Fig. S1b†), a flat and continuous stacked nanosheet-like morphology (Fig. 2a) firstly changes rough (Fig. 2b and 2c), then becomes tiny fragments (Fig. 2d and 2e), and lastly forms a highly open and porous structure (Fig. 2f-2h) with increasing the molar ratios of NH_4HSO_4/MnO_2. When the molar ratio of NH_4HSO_4/MnO_2 is 2.1, very tiny and disordered primary nanocrystals with a size of about 5 nm are observed for the obtained material. XRD patterns and TEM images indicate that the amount of NH_4HSO_4 plays a crucial role in the formation of mesoporous-assembled MnO_2.

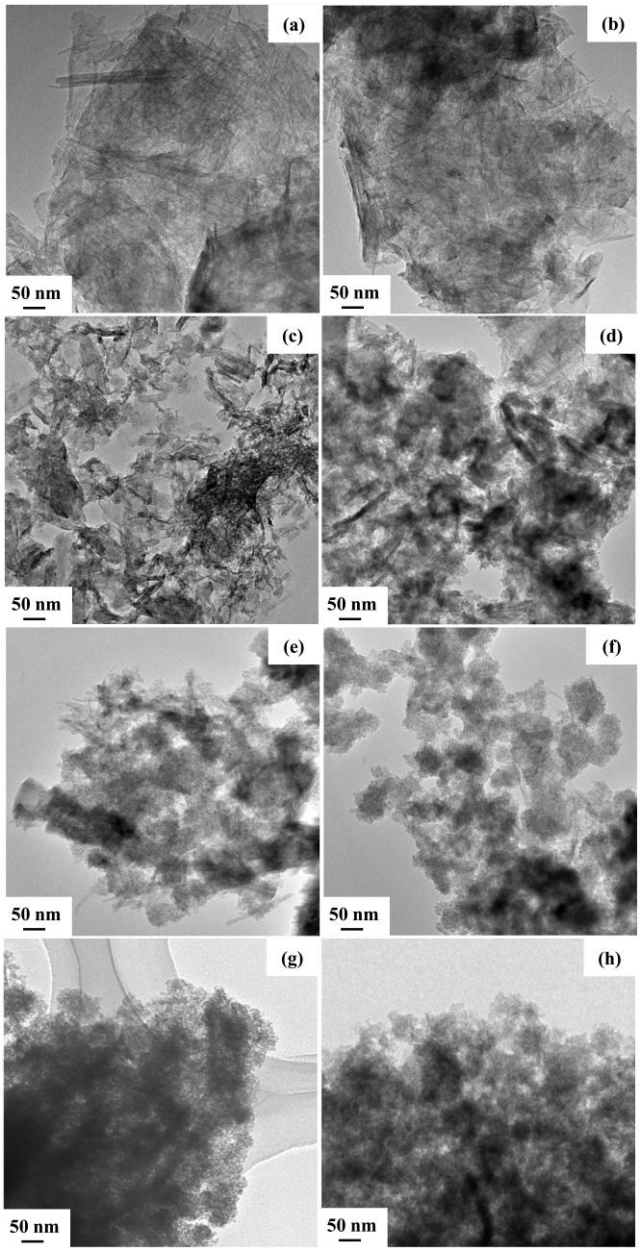

Fig. 2 TEM images of the mesoporous-assembled MnO_2 with different molar ratios of NH_4HSO_4/MnO_2: (a) 0, (b) 0.1, (c) 0.2, (d) 0.4, (e) 0.7, (f) 1.4, (g) 2.1, and (h) 2.8, respectively.

The porosity of the obtained materials with different molar ratios of NH_4HSO_4/MnO_2 is characterized by N_2 adsorption-desorption isotherm (Fig. 3). For the material obtained from calcining the delaminated manganese oxide slurry at 175 °C for 5 h, the N_2 adsorption-desorption isotherm shows a typical type IV isotherm. A hysteresis loop of N_2 adsorption and desorption branches

occurs at the relative pressure (P/P_0) between 0.40 and 1.0, indicating the existence of mesopores. The BET specific surface area is 47 m^2 g^{-1} and the pore size distribution centers at around 3.8 nm as calculated by the NLDFT model (inset in Fig. 3). In accompany with the molar ratio of NH_4HSO_4/MnO_2 increase (0-0.4), N_2 adsorption-desorption isotherms of the obtained materials nearly maintains the type IV characteristics with distinct hysteresis loops observed at a relative pressures (P/P_0) between 0.4 and 1.0. When the molar ratio of NH_4HSO_4/MnO_2 is larger than 0.7, an obvious IV characteristics isotherm with two small hysteresis loops are observed. One is a small hysteresis loop occurs at the relative pressure (P/P_0) between 0.4 and 0.8, which is related to the filling and emptying of mesopores by capillary condensation. And the other is an obvious increasing step of the nitrogen adsorption volume at the relative pressure higher than 0.9, suggesting the presence of secondary pores due to the aggregation of particles with uniform size.[19] Moreover, a new pore size distribution at around 1.5 nm is observed except the pore size distribution between 2.5-4.0 nm, further supporting the micropore presence of secondary pores.

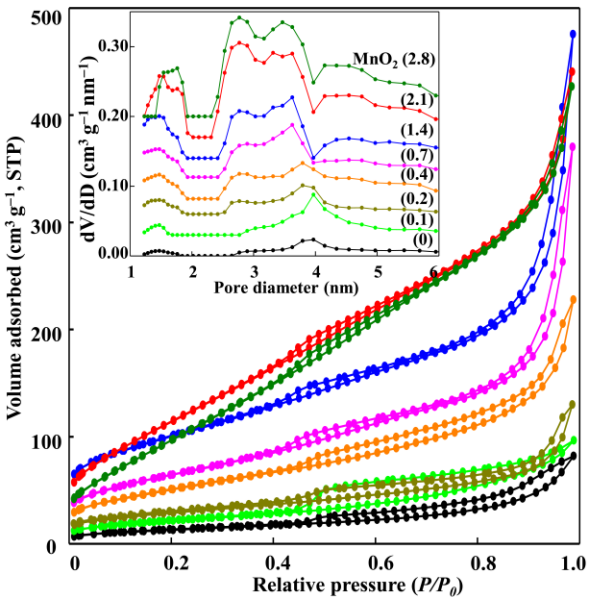

Fig. 3 Nitrogen adsorption-desorption isotherms of the mesoporous-assembled MnO_2 with different molar ratios of NH_4HSO_4/MnO_2, and NLDFT pore size distribution curves are inserted.

The textural parameters of the obtained materials with different molar ratios of NH_4HSO_4/MnO_2 are summarized in Table 1. It can be seen that both the specific surface area and the pore volume significantly increase with the increase of the molar ratios. MnO_2 (2.1) shows the largest surface area of 456 m^2 g^{-1} and the higher total pore volume of 0.68 cm^3 g^{-1}. However, further increase amount of NH_4HSO_4 leads to a decrease in surface area and pore volume, which is probably ascribed to the aggregated structure caused by stacking and overlapping of MnO_2 nanoparticles. These results indicate that the worse the crystalline nature of the obtained materials, the larger the specific surface area. NH_4HSO_4 plays an important role in the formation of nanostructured MnO_2 with reduced size, and the optimized molar ratio of NH_4HSO_4/MnO_2 is 2.1.

Table 1 The specific surface area, manganese oxidation state, and the capacitance of the obtained MnO_2 with different molar ratios of NH_4HSO_4/MnO_2.

Samples (NH_4HSO_4/MnO_2)	S_{BET}[a] (m^2 g^{-1})	D_{DFT}[a] (nm)	V_{total}[a] (cm^3 g^{-1})	Mn[b] oxidation state	Capacitance[c] (F g^{-1})	Capacitance retention (%)
MnO_2 (0)	47	4.0	0.13	3.43	124	33.1
MnO_2 (0.1)	77	4.0	0.15	3.50	145	37.9
MnO_2 (0.2)	101	3.8	0.20	3.54	179	39.1
MnO_2 (0.4)	184	3.8	0.35	3.61	198	41.4
MnO_2 (0.7)	231	3.6	0.57	3.67	235	49.8
MnO_2 (1.4)	350	3.6	0.74	3.71	273	53.1
MnO_2 (2.1)	456	2.8	0.68	3.80	281	54.8
MnO_2 (2.8)	421	2.8	0.66	3.81	278	55.0

[a] BET surface area and NLDFT pore diameter obtained from the desorption branches of the N_2 adsorption/desorption isotherm. The total pore volume was estimated at P/P_0=0.99. [b] Mn valence state obtained from the linear relationship between the energy separation of the Mn 3s peaks and Mn oxidation state of manganese oxides. [c] Capacitance obtained from the galvanostatic discharge process at current density of 0.25 A g^{-1}.

In order to further understand how the specific surface area changes and how the reaction process carries out with the extention of molar ratio, the Mn 2p and Mn 3s XPS spectra of the obtained materials with different molar ratios of NH_4HSO_4/MnO_2 are conducted and the results are shown in Figure 4. For the Mn 2p core level spectrum, two peaks at about 642.2 and 654.0 eV are observed, which correspond to the binding energies of Mn 2p3/2 and Mn 2p1/2 (Fig. 4a). The binding energy values agree well with those of the prepared MnO_2,[20] suggesting that a large number of Mn (IV) are existed in the obtained nanostructured MnO_2. It can be seen that the corresponding binding energy gradually shifts to the higher energy with the molar ratio increase of NH_4HSO_4/MnO_2, suggesting that Mn valences of the obtained nanostructured MnO_2 increases gradually.

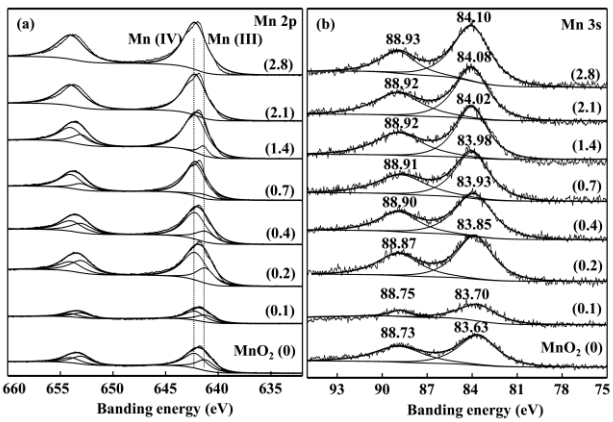

Fig. 4 Mn 2p (a) and Mn 3s (b) core level spectra of the mesoporous-assembled MnO_2 with different molar ratios of NH_4HSO_4/MnO_2.

To obtain further information why the manganese oxidation state gradually increases in the obtained nanostructured MnO_2, the Mn 2p3/2 peaks are fitted using Gaussian functions to achieve the relative intensities of the component. It can be seen that the Mn 2p3/2 spectra can be separated into two peaks. The deconvoluted peaks are centered at 642.2 and 641.2 eV, suggesting that the valence of the Mn ions is +4 and +3, respectively. In addition, the peak intensity of Mn (IV) species gradually increases, while it

gradually decreasas for Mn (III) species in accompany with the molar ratio of NH_4HSO_4/MnO_2 increase. It is insufficient to determine exactly the manganese oxidation state only from the Mn 2p spectrum, and more important information may be further obtained from Mn 3s core level spectrum (Fig. 4b). According to the relationship between the energy separation of Mn 3s peaks and Mn oxidation state of manganese oxides,[21] the Mn oxidation valence of the obtained nanostructured MnO_2 indeed increases with the molar ratio increase (Table 1). The increase of the mean manganese oxidation number is probably due to a disproportionation reaction of some Mn (III) ($Mn^{III} \rightarrow Mn^{II} + Mn^{IV}$) in the acid condition obtained from NH_4HSO_4 ($H_2SO_4 + NH_3 \leftrightarrow H_2SO_4 \cdot NH_3$).[22] Mn (III) derived from two sources, one is the mixed-valent manganese framework,[23] and the other is the redox reaction between H_2SO_4 and MnO_2 ($4H_2SO_4 + 6MnO_2 = 2Mn_2(SO_4)_3 + 6H_2O + O_2\uparrow$) in the heating process.[24] The XPS data in consistent with the above mentioned XRD results, further corroborate the obtained materials are primarily composed of MnO_2 with little amount of Mn (III) species.

The formation process of mesoporous-assembled MnO_2 probably consists of the ion exchange (TMA^+/NH_4^+) and redox reaction processes (Mn^{4+} to Mn^{3+}). When little amount of NH_4HSO_4 is used in the reaction system ($NH_4HSO_4/MnO_2 < 0.7$), the TMA^+ ions are exchanged with NH_4^+ ones, causing the basal spacing decrease from 0.96 to 0.73 nm. However, when the excessive amount of NH_4HSO_4 ($NH_4HSO_4/MnO_2 > 0.7$-2.8) exist in the system, the manganese oxide are reduced, which causes the collapse of manganese oxide framework and forms mesoporous-assembled MnO_2. In addition, the similar experimental results are observed when NH_4HSO_4 are replaced by H_2SO_4 treatment (Fig. S2†).

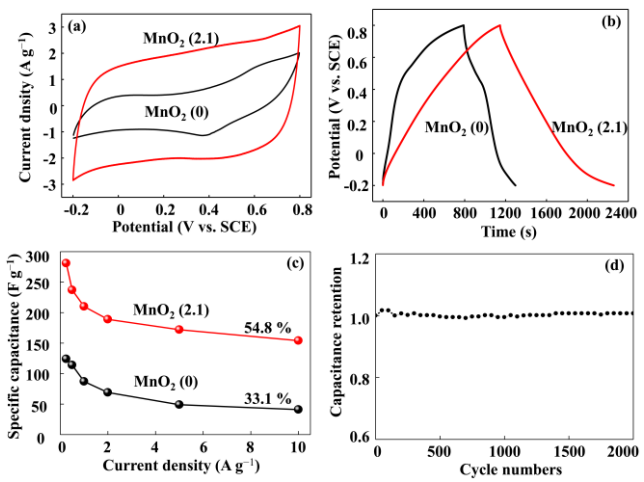

Fig. 5 Electrochemical characterization of MnO_2 (0) and MnO_2 (2.1): (a) CV curves at a scan rate of 10 mV s^{-1}, (b) charge-discharge curves at a current density of 0.25 A g^{-1}, (c) Capacitance retention at different current densities, and (d) Cycling performance of MnO_2 (2.1) at a current density of 2 A g^{-1} for 2000 cycles.

In general, the specific capacitance of the electrode material is related to its specific surface area, the electrical conductivity in the solid phase and ionic transport within the pores. The large specific surface area and good ionic transport can lead to a higher capacitance and facilitate the fast transport of electrolyte ions.[25]

The electrochemical performance of the obtained nanostructured MnO_2 (0) and MnO_2 (2.1) electrodes was evaluated by a three-electrode system between −0.2 and 0.8 V in 1 mol L^{-1} Na_2SO_4 electrolyte.

The cyclic voltammetry (CV) curve of MnO_2 (0) electrode is distorted and have a pair of redox peaks, which is ascribed to a Faradic pseudocapacitance due to the intercalation/detercalation of protons or alkaline metal cations in MnO_2 (0) electrode. In contrast, the CV curve of MnO_2 (2.1) electrode exhibits much larger enclosed areas and a quasi-rectangular shape with a mirror image feature (Fig. 5a), indicating the ideal electrical double-layer capacitance behavior and fast charging-discharging process characteristic.[26] Morever, its galvanostatic charge/discharge curve shows that the specific capacitance is 281 F g^{-1} at 0.25 A g^{-1}, which is higher than that of MnO_2 (0) electrode (124 F g^{-1}) (Fig. 5b) and other MnO_2 (x) electrodes (Fig. S3†). The specific capacitance is also higher than the values of some porous MnO_2 nanostructures reported in the literatures, such as porous MnO_2 with a 3D framework (218 F g^{-1}, 0.1 A g^{-1}),[27] three-dimensional ordered macroporous MnO_2/carbon nanocomposites (234 F g^{-1}, 0.1 A g^{-1}),[28] and flower-like hierarchical α-MnO_2 sub-microspherical superstructures constructed by two-dimension mesoporous nanosheets (298 F g^{-1}, 0.117 A g^{-1}).[29] With the molar ratio of NH_4HSO_4/MnO_2 increase, the specific capacitance of the obtained materials increases gradually (Table 1). More importantly, the MnO_2 (2.1) electrode also shows a higher rate capability compared with that of MnO_2 (0) electrode and other MnO_2 (x) electrodes (Fig. S4†). Even at 10 A g^{-1}, it still retains 154 F g^{-1} (about 54.8%, Fig. 5c). The better rate performance are probably ascribed to its larger surface area and mesoporous structure, which facilitate the improvement of kinetics due to the increased reaction interface and the reduced diffusion path for ionic intercalation and deintercalation.[8] In addition, the long-term cycle stability is evaluated by repeating the galvanostatic charge/discharge test at a current density of 2 A g^{-1} for 2000 cycles (Fig. 5d), there is only 1.9% specific capacitance loss, suggesting that the MnO_2 (2.1) electrode shows good electrochemical cycle stability. Nyquist plots of MnO_2 (2.1) electrode before and after 2000 cycles at the frequency range from 100 kHz to 0.01 Hz show similar equivalent series resistance (ESR) of about 2 Ω and diffusion resistance, indicating that the MnO_2 (2.1) electrode has good capacitive behavior (Fig. S5†).

Conclusions

In summary, the mesoporous-assembled MnO_2 with large specific surface area of 456 m^2 g^{-1} is prepared by heating the delaminated MnO_2 nanosheet slurry with NH_4HSO_4 at 175 °C. The molar ratio of NH_4HSO_4/MnO_2 plays an crucial role in the formation of the mesoporous-assembled MnO_2 with larger specific surface area, and the optimized molar ratio of NH_4HSO_4/MnO_2 is 2.1. The as-fabricated nanostructured MnO_2 electrode delivers the specific capacitance of 281 F g^{-1} at a current density of 0.25 A g^{-1} and excellent cycling performance. This novel preparation method can be used to prepare the other nanostructured transition metal oxides with large specific surface area, and they can be used as energy storage materials, catalysts, adsorbents, and so on.

Acknowledgements

This work was financially supported by the National Natural Science Foundation of China (51172137, 21471093), the Program for Key Science & Technology Innovation Team of Shaanxi Province (2012KCT-21), the 111 Project, and the Fundamental Research Funds for the Central Universities (GK201301002 and GK201501007).

Notes and references

Key Laboratory of Applied Surface and Colloid Chemistry (Shaanxi Normal University), Ministry of Education, Xi'an 710062, P.R. China, School of Materials Science and Engineering, Shaanxi Normal University, Xi'an 710062, P.R. China. Fax: ++86-29-8153 0702; Tel: ++86-29-8153 0706; E-mail: zhliu@snnu.edu.cn

† Electronic Supplementary Information (ESI) available: Experimental details, characterization, electrochemical measurements and additional figures. See DOI: 10.1039/b000000x/

1 C. K. King'ondu, A. Iyer, E. C. Njagi, N. Opembe, H. Genuino, H. Huang, R. A. Ristau and S. L. Suib, *J. Am. Chem. Soc.*, 2011, **133**, 4186−4189.

2 Y. Gorlin, B. Lassalle-Kaiser, J. D. Benck, S. Gul, S. M. Webb, V. K. Yachandra, J. Yano and T. F. Jaramillo, *J. Am. Chem. Soc.*, 2013, **135**, 8525−8534.

3 Y. H. Teng, Y. Kusano, M. Azuma, M. Haruta and Y. Shimakawa, *Catal. Sci. Technol.*, 2011, **1**, 920−922.

4 W. F. Wei, X. W. Cui, W. X. Chen and D. G. Ivey, *Chem. Soc. Rev.*, 2011, **40**, 1697−1721.

5 G. H. Yu , L. B. Hu, M. Vosgueritchian, H. L. Wang, X. Xie, J. R. McDonough, X. Cui, Y. Cui and Z. N. Bao, *Nano Lett.*, 2011, **11**, 2905−2911.

6 J. J. Shao, X. Y. Zhou, Q. Liu, R. J. Zou, W. Y. Li, J. M. Yang and J. Q. Hu, *J. Mater. Chem. A*, 2015, **3**, 6168−6176.

7 G. P. Wang, L. Zhang and J. J. Zhang, *Chem. Soc. Rev.*, 2012, **41**, 797−828.

8 K. Zhang, X. P. Han, Z. Hu, X. L. Zhang, Z. L. Tao and J. Chen, *Chem. Soc. Rev.*, 2015, **44**, 699−728.

9 X. H. Tang, Z.-H. Liu, C. X. Zhang, Z. P. Yang and Z. L. Wang, *J. Power Sources*, 2009, **193**, 939−943.

10 S. Chen, G. X. Liu, H. Yadegari, H. H. Wang and S. Z. Qiao, *J. Mater. Chem. A*, 2015, **3**, 2559−2563.

11 H. Jiang, T. Sun, C. Z. Li and J. Ma, *J. Mater. Chem.*, 2012, **22**, 2751−2756.

12 G. Zhu, L. J. Deng, J. F. Wang, L. P. Kang and Z.-H. Liu, *Mater. Res. Bull.*, 2012, **47**, 3533−3537.

13 C.-W. Lee, S.-B. Yoon, S.-M. Bak, J. Han, K. C. Roh and K.-B. Kim, *J. Mater. Chem. A*, 2014, **2**, 3641−3647.

14 B. Zhi, H. Ding, D. M. Wang, Y. Cao, Y. Zhang, X. Wang, Y. L. Liu and Q. S. Huo, *J. Mater. Chem. A*, 2014, **2**, 2374−2382.

15 S. Ching, I. J. Richter, K. A. Tutunjian, D. A. Kriz and Y. Kovic, *Chem. Commom.*, 2015, **51**, 1961−1964.

16 Z.-H. Liu, K. Ooi, H. Kanoh, W.-P. Tang and T. Tomida, *Langmuir*, 2000, **16**, 4154−4164.

17 Z.-H. Liu, X. J. Yang, Y. Makita and K. Ooi, *Chem. Mater.*, 2002, **14**, 4800−4806.

18 M. Nakayam, M. Fukuda, S. Konishi and T. Tonosaki, *J. Mater. Res.*, 2006, **21**, 3152−3160.

19 G. J. Zhang, Z. R. Shen, M. Liu, C. H. Guo, P. C. Sun, Z. Y. Yuan, B. H. Li, D. T. Ding and T. H. Chen, *J. Phys. Chem. B*, 2006, **110**, 25782−25790.

20 J. X. Lin, Y. Y. Zheng, Q. F. Du, M. P. He and Z. W. Deng, *NANO*, 2013, **8**, 1350004 (8 pages).

21 C. Wei, L. H. Yu, C. L. Cui, J. D. Lin, C. Wei, N. Mathews, F. W. Huo, T. Sritharan and Z. C. Xu, *Chem. Commun.*, 2014, **50**, 7885−7888.

22 T. Kurten, M. R. Sundberg, H. Vehkamaki, M. Noppel, J. Blomqvist and M. Kulmala, *J. Phys. Chem. A*, 2006, **110**, 7178−7188.

23 X.-F. Shen, Y.-S. Ding, J. Liu, J. Cai, K. Laubernds, R. P. Zerger, A. Vasiliev, M. Aindow and S. L. Suib, *Adv. Mater.*, 2005, **17**. 805−809.

24 Y.-M. Yang and M. Deng, *Journal of China West Normal University (Natural Sciences)*, 2007, **28**, 94−98.

25 A. S. Aricò, P. Bruce, B. Scrosati, J.-M. Tarascon and W. Van Schalkwijk, *Nat. Mater.*, 2005, **4**, 366−377.

26 P. Simon and Y. Gogotsi, *Nat. Mater.*, 2008, **7**, 845−854.

27 X. Y. Xie, C. Zhang, M.-B. Wu, Y. Tao, W. Lv and Q.-H. Yang, *Chem. Commun.*, 2013, **49**, 11092−11094.

28 C. Z. Yang, M. Zhou and Q. Xu, *Phys. Chem. Chem. Phys.*, 2013, **15**, 19730−19740.

29 C. Z. Yuan, L. R. Hou, L. Yang, D. K. Li, L. F. Shen, F. Zhang and X. G. Zhang, *J. Mater. Chem.*, 2011, **21**, 16035−16041.

TOC

The mesoporous MnO_2 with surface area of 456 m^2/g is prepared by heating the delaminated MnO_2 nanosheet slurry with NH_4HSO_4.